



COMPARATIVE MODELING OF IONS AND SOLVENT PROPERTIES IN Ca-Na MONTMORILLONITE BY ATOMISTIC SIMULATIONS AND FLUID DENSITY FUNCTIONAL THEORY

GUOMIN YANG^{1*} , NIKOLAOS I. PRASIANAKIS¹, AND SERGEY V. CHURAKOV^{1,2}

¹Laboratory for Waste Management, Paul Scherrer Institute, 5232 Villigen, PSI, Switzerland

²Institute of Geological Sciences, University of Bern, Baltzerstrasse 1+3, Room 121, CH-3012 Bern, Switzerland

Abstract—Molecular dynamics (MD) simulations provide an accurate description of the mineral–fluid interface from the perspective of the atomistic level taking into account all atom interactions. This simulation approach is computationally expensive if applied to large molecular systems. Classical Fluid Density Functional Theory (f-DFT) delivers structural and thermodynamic information at comparatively small computational costs. Numerous applications of f-DFT for electrolytes neglect an explicit consideration of solvent. In this work, an unrestricted three-component model (3CM) of f-DFT was applied, which incorporates Lennard-Jones (LJ) attractions for the description of the short-range interactions of fluid–fluid and fluid–wall rather than the hard sphere repulsions, named DFT/LJ-3CM. The DFT/LJ-3CM model considers ions as charged LJ particles and treats solvent molecules as neutral LJ particles. To validate the performance of the DFT/LJ-3CM, the f-DFT calculations were compared with atomistic simulations for montmorillonite (Mnt) with various hydrated states in electrolyte solutions. This benchmarking was used to assess critically the advantages and limitations of the f-DFT model. The calibrated DFT/LJ-3CM model for Na and Ca Mnt was applied to calculate cation selectivity for the ion exchange equilibrium with effective ion radius and swelling behavior of Mnt. The predictions of the DFT/LJ-3CM model were found to be in good agreement with the atomistic simulations and experimental data under a wide range of conditions. At the same time, the DFT calculations were 3–4 orders of magnitude faster than conventional MD simulations. Thus, the DFT/LJ-3CM model can be a computationally effective alternative to atomistic simulation in providing structural and thermodynamic properties of fluid–clay mineral interfaces. The DFT/LJ-3CM model provides a robust approach, which can be used for upscaling in reactive transport simulators and modeling ion migration taking place under more complex thermo-chemo-hydro-mechanical conditions.

Keywords—Clay minerals · Fluid density functional theory · Molecular dynamics · Solvent effects

INTRODUCTION

Clay minerals are composed of permanently charged platelets with equivalent spherical diameter $<2\ \mu\text{m}$ (Schoonheydt & Johnston 2006). Because of the high surface charge and the large surface area, clay minerals possess high sorption and pH buffering capacity (Bloom 2000). Hydration of charge-compensating interlayer cations in clay minerals leads to swelling and diffusive migration of water molecules and cations. Due to the low hydraulic conductivity and self-sealing properties related to swelling, clays are used as efficient hydraulic barriers to contain migration of hazardous contaminants (Lo et al. 1997; Edil 2003; Rowe 2005). For instance, Opalinus Clay (Switzerland) is proposed as a potential host rock for geological waste disposal (Marschall et al. 2005). Bentonite is used as a sealing material in the Swedish waste disposal concept for high-level radioactive waste (SKB 2006). Clay cap-rocks are used for carbon storage and sequestration (Song & Zhang 2013).

The hydraulic permeability of compacted argillaceous rocks is extremely low. Molecular diffusion is the dominant transport mechanism of solute and solvent in these materials. Several experimental observations provide clear evidence that

the surface adsorbed cations in compacted clays are not fully immobilized and contribute to the overall diffusive flux (van Schaik et al. 1966; Eriksen et al. 1999; Melkior et al. 2005, 2007; Van Loon & Eikenberg 2005; Gimmi & Kosakowski 2011). The mechanism and the importance of surface diffusion in argillaceous rock is still under debate (Bourg et al. 2003). Effective macroscopic transport in porous media depends on a number of geometrical and electrochemical parameters. The pore network connectivity, tortuosity, and pore-size distribution are the geometric constraints controlling mass transport (Tyagi et al. 2013; Churakov et al. 2014; Gimmi & Churakov 2019). The interaction of ions with the charged mineral surfaces leads to the formation of so-called diffuse double layers (DDL). For negatively charged clay minerals, the DDL is enriched in cations and depleted in anions. The mobility of cations within the DDL has been shown to be reduced due to electrokinetic phenomena and the steric interaction of ions with clay mineral surfaces (Rotenberg et al. 2007a, b; Pagonabarraga et al. 2010; Botan et al. 2011; Obliger et al. 2013, 2014; Schaettle et al. 2018). In order to model accurately water and cation diffusion in a reactive transport environment, the effect of DDL (Alt-Epping et al. 2018) and pore network geometry need to be taken into account simultaneously.

Macroscopic reactive transport models (Yang et al. 2019) integrate such complex phenomena in a very simplistic way; e.g. using the Poisson-Boltzmann equation to describe the properties of a mineral–fluid interface. The Poisson-

* E-mail address of corresponding author: guomin.yang@psi.ch
DOI: 10.1007/s42860-019-00058-5

Boltzmann equation is based on the assumption that the ions are point charges embedded in a uniform dielectric continuum and, thus, the molecular nature of solvent and finite ionic size are completely ignored. Consequently, macroscopic models break down, especially when the interlayer space or water content is very small (Rotenberg et al., 2007a, b) or at high surface charge density and high ionic strength.

In contrast to simplified macroscopic models, molecular simulations such as Monte Carlo (MC) (Torrie & Valleau 1980; Boda et al. 2004; Silvestre-Alcantara et al. 2016) and molecular dynamics simulations (MD) (Chang et al. 1998; Marry et al. 2008; Holmboe & Bourg 2014; Yang et al. 2017b) take the finite size of molecular solvent and ions and, most relevant, the interatomic interactions of the system into account (Kosakowski et al. 2008; Churakov & Gimmi 2011; Churakov 2013; Prasianakis et al. 2017). However, they are computationally expensive for the description of mineral–fluid interactions if large systems need to be considered. Classical density functional theory (DFT) (Henderson 1992; Hansen & McDonald 2006; Yang & Liu 2015; Yang et al. 2016, 2017a) at the atomistic level has been used widely to describe the mineral–fluid interfaces because it provides a computationally inexpensive alternative. Numerical modeling based on classical DFT can easily handle molecular systems two to three orders of magnitude larger than one considered in MC and MD simulations. Classical DFT has difficulty taking into account hydrogen bonding between water molecules and the surface of the clay mineral (Sposito 1984) and describing specific orientation-dependent distributions of the interfacial water molecules hydrating the surface and the interlayer ions (Marry et al. 2008). Recently, Borgis and coworkers proposed a DFT for SPC/E water, which has been used to study pyrophyllite (Jeanmairet et al. 2014).

Various models have been proposed within the framework of classical DFT to take into account the solvent effects. For example, early work (Tang et al. 1992, Lamperski & Zydor 2007) introduced the solvent primitive model i.e. a three-component model (3CM or the so called DFT/HS-3CM), in which the solvent molecules are represented by neutral hard spheres (HS) on the basis of the simplest restricted primitive model (Yang et al. 2016, 2017a) (RPM or the so called DFT/HS-2CM), where the ions of electrolytes with the same size are modeled by hard spheres with point charges located at their centers, the electrode by a uniformly charged surface, and the solvent by a uniform dielectric continuum. Comparison between the RPM and the 3CM models showed that the solvent plays a significant role in the solid–fluid interfacial properties (Lamperski & Zydor 2007). Later, the 3CM model was validated (Lee et al. 2013) by comparison with the molecular solvent model (Jorgensen et al. 1983; Price & Brooks 2004) in which solvents and ions were described explicitly as distinct atoms, using MD simulations. However, most of the insights into the solvent arrangement could not be provided by the 3CM model, notwithstanding the fact that the density distributions and other interfacial properties were qualitatively captured by such a coarse-grained model. Lee et al. (2012), therefore, introduced a modified 3CM which incorporated

Lennard-Jones attractions into the fluid–fluid and fluid–wall interactions rather than the hard-sphere and hard-wall repulsions. Other DFT studies of electrolytes in solution also used solvent modes. For instance, Oleksy & Hansen (2010) proposed wetting a solid substrate by a “civilized” model of ionic solutions, in which water is described by dipolar hard spheres. Lian et al. (2017) investigated electrostatic energy extraction by few-layer graphene electrodes, where the solvent is described by hard sphere dimers with opposite charges.

Many attempts have been made to reproduce the properties of interfacial water layers as revealed by molecular simulations and experimental observations (Fenter et al. 2000; Schlegel et al. 2006) using simplified theories from the perspective of a macroscopic scale (Qiao & Aluru 2003; Toumassat et al. 2009; Botan et al. 2013). An advanced Grand Canonical Monte Carlo (GCMC) technique was used (Moucka et al. 2017) to model pyrophyllite and Na-Mnt in equilibrium with a bulk solution having salt concentrations of 3.14 and 6.6 mol kg⁻¹ with pore size ranging from ~7 to 28 Å. This GCMC technique is based on fractional exchanges of dissolved ions and water molecules. The chemical potentials of NaCl and water in the bulk phase were determined using Osmotic Ensemble Monte Carlo simulations. The chemical potential was then used in GCMC to simulate the adsorption of ions and water molecules in the clay pores, and in turn to predict the salt solubility in confined solutions.

The present work was motivated by the GCMC and the merits of the modified 3CM model, which can be implemented numerically by classical DFT, to describe the structure and interfacial properties by explicitly taking into account the solvent effects, yet in a simplified form. Atomistic simulations reveal clearly that water molecules play an important role in saturated (Holmboe & Bourg 2014) or partially saturated clay systems (Churakov 2013). Therefore, theoretical methods at the atomic level such as classical DFT take into account water molecules for mineral–fluid interfaces. To this end, the objective was to validate the DFT/LJ-3CM of modeling structures of water molecules and ions in Mnt interlayers by atomistic simulations under a wide range of conditions, to compare systematically the new DFT approach with the structural data obtained by MD simulations, and then to test thermodynamic properties of the model with respect to the swelling behavior of clay systems and ion exchange as a function of water content, ionic strength of electrolyte (1:1, 2:1 salts), and temperature.

METHODS AND MODELS

System Setup for Molecular Simulations

A periodic 3D supercell containing two fully flexible Mnt layers was set up according to the previous modeling studies of hydrated Mnt (Skipper et al. 1995a,b; Tambach et al. 2004; Toumassat et al. 2009; Bourg and Sposito 2011; Holmboe & Bourg 2014; Marry et al. 2008). A single TOT (2:1 tetrahedral-octahedral-tetrahedral) layer in the simulation supercell consisted of 6×6×1 unit cells of Mnt. The supercell dimensions in the direction perpendicular to the basal plane were adjusted to accommodate the appropriate number of water molecules in

the interlayer to simulate the hydration state of Mnt. The Mg-for-Al isomorphous substitutions in the octahedral sheet were distributed randomly, but excluded Mg-Mg pairs to maintain a mean layer surface charge density of -0.116 C/m^2 , consistent with previous MD simulations (Tournassat et al. 2009). A representative snapshot (Fig. 1) shows the simulation supercell of Na-Mnt in the 5W hydration state with z dimension 50.8 \AA , containing 52 Na ions, 4 Cl ions, and 1800 H_2O water molecules. In the following discussion, the interlayer size is defined as the distance between the basal planes of the outermost oxygen atoms of Mnt.

Classical MD Simulations

MD simulations were performed using the open source package *GROMACS* (Berendsen et al. 1995; van der Spoel et al. 2005) which uses the *CLAYFF* force field (Cygan et al. 2004) for montmorillonite, the ion-potentials reported by Åqvist (1990) for Ca^{2+} , Joung-Cheatham parameters (Joung & Cheatham III 2008) for monovalent ions (Na^+/Cl^-), and the SPC/E water model (Berendsen et al. 1987) for all interatomic interactions. The Lennard-Jones shift potential was truncated beyond a cutoff value of 1.0 nm . The long-range electrostatic interactions were computed using the Particle-Mesh-Ewald (PME) method (Darden et al. 1993). All atomic simulations were conducted at 298 K using a time step of 1 fs . The integration of the equations of motion was performed using the leap-frog algorithm. Energy minimization with the steepest descent algorithm was used to prepare the initial configurations. The equilibration was performed in two steps. First, the system was pre-equilibrated in the NPT ensemble (pressure P , number of particles N , and temperature T were fixed) for 5 ns using the Berendsen barostat (Berendsen et al. 1984) at 298 K

and 1 bar to relax the Mnt layers and interlayer electrolytes in all the dimensions. The 5 ns -long NVT (fixed volume V , N , and T) runs were performed using position restraints of the clay lattices to generate equilibrated systems. The x and y dimensions of the NVT supercell in all simulated hydration states were kept at $31.0 \text{ \AA} \times 54.2 \text{ \AA}$. The dimensions of the supercell in the z direction and the composition of the interlayer are given in Table 1. The production runs were performed for 125 ns in the NVT ensemble at 298 K .

Fluid DFT Calculations

The f-DFT simulations were conducted using the open source package *Tramonto* developed at Sandia National Laboratories (<https://software.sandia.gov/tramonto/>). The f-DFT simulations were performed in grand canonical ensemble (μVT), where the total volume V , the temperature T , and the chemical potentials μ of the system were kept constant. Classical MD used in this study was implemented in the NVT ensemble. Therefore, the assignment of a consistent setup for f-DFT and MD simulations and μVT and NVT ensembles was not trivial. To match the condition of f-DFT and MD simulations two different approaches for the system were used at low (< 5 water layers) and high (≥ 5 water layers) degrees of hydration. At low degrees of hydration, the total number of ionic species and water molecules in the interlayer space were set to be the same in both f-DFT and MD systems. At high degrees of hydration the chemical potential in f-DFT was set to match the density representing the regions of homogeneous fluid in the central part of the interlayer space.

In f-DFT, the density distributions of molecular species of fluid at equilibrium, $\rho_i(\mathbf{r})$, were determined by minimization of the grand potential energy at equilibrium described by the

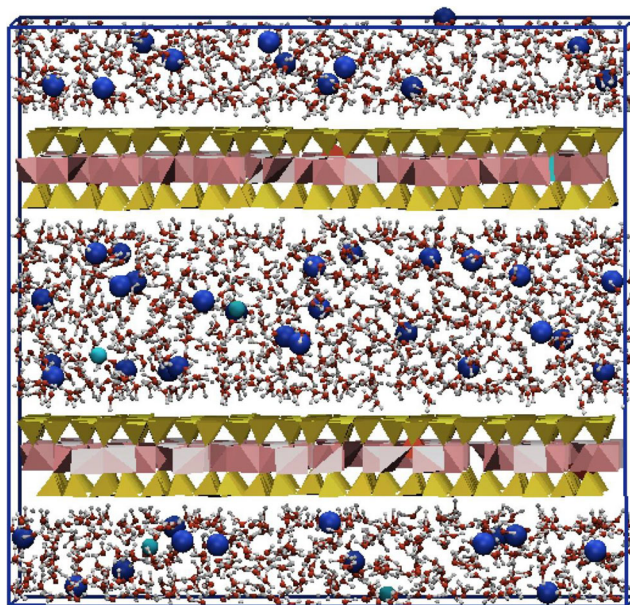


Fig. 1. Snapshot of a MD simulation cell showing Na-Mnt in the 5W hydration state with z dimension 50.8 \AA containing Na ions (dark blue), Cl ions (light blue), and water molecules (O and H atoms are in red and white, respectively). The clay layer consists of an octahedral sheet (pink) sandwiched by tetrahedral sheets (gold yellow)

Table 1. Simulation parameters of the supercell for the MD simulations

Simulation parameter of the supercell	Hydration State			
	2W	3W	4W	5W
Dimension in z -direction \AA	31.33	38.42	44.46	50.83
Number of Na ions	50	52	52	52
Number of Cl ions	2	4	4	4
Number of water molecules	720	1080	1440	1800

Euler-Lagrange equation. The chemical potential was expressed as a function of the external potential, Coulomb forces, ideal gas components, and excess energy due to hard-sphere repulsions (f_i^{hs}), Lennard-Jones attractions (f_i^{LJ}), and short-range electrostatic interactions (f_i^{MSA}) were evaluated with the Mean Spherical Approximation (MSA) (Waisman & Lebowitz 1972):

$$\mu_i(\mathbf{r}) = q_i e \psi(\mathbf{r}) + u_i(\mathbf{r}) + kT \ln \rho_i(\mathbf{r}) + f_i^{hs}(\mathbf{r}) + f_i^{LJ}(\mathbf{r}) + f_i^{MSA}(\mathbf{r}) \quad (1)$$

in which $\psi(\mathbf{r})$ is the local electrostatic potential resulting from the Coulombic interaction between point charges and that from the electrostatic part of the external potential, which was obtained by solving Poisson's equation, q_i is the valence of the ionic species i using the expression

$$\nabla^2 \psi(\mathbf{r}) = -\frac{1}{\epsilon_0 \epsilon_r} \sum_i \rho_i(\mathbf{r}) e z_i \quad (2)$$

where ϵ_0 is the vacuum permittivity, ϵ_r is the relative permittivity or dielectric constant, z_i is the valence of the ionic species i , and e is the elementary charge. The external field, $u_i(\mathbf{r})$, is induced by the clay surface, which is described as a flat wall with surface charge density σ uniformly distributed on the surface, k is Boltzmann's constant, T is the absolute temperature, and $f_i(\mathbf{r})$ is the Helmholtz free energy per molecule of the particle i .

The one-dimensional external potential due to the wall–fluid interaction was represented by the Lennard-Jones 9-3 potential:

$$\mu_i(z) = \epsilon_{wf}^{LJ} \left[\frac{2}{15} \left(\frac{d}{z} \right)^9 - \left(\frac{d}{z} \right)^3 \right] \quad (3)$$

where ϵ_{wf}^{LJ} is the LJ energy interaction parameter for wall–fluid interaction potential, d is the LJ particle diameter, and z is the position of molecular particle i from the wall in the direction perpendicular to the wall. The wall–fluid potential cutoff was set at $3.5 d$.

The LJ interaction is described in a spirit of perturbation theory as hard-sphere interaction with an effective hard-sphere parameter d and the correction due to long-range interactions (Tang et al. 1991). The hard-sphere component, $f_i^{hs}(\mathbf{r})$, was calculated using the fundamental measure theory (FMT) developed by Rosenfeld (1989). The short-range interaction cutoff for $f_i^{hs}(\mathbf{r})$ was $1d$. The excess free energy was based on the following formula,

$$f_i^{hs}(\mathbf{r}) = -n_0 \ln(1-n_3) + \frac{n_1 n_2 - \mathbf{n}_{v1} \cdot \mathbf{n}_{v1}}{1-n_3} + \frac{1}{24\pi} \frac{n_2^3}{(1-n_3)^2} - \frac{1}{8\pi} \frac{n_2 (\mathbf{n}_{v2} \cdot \mathbf{n}_{v2})}{(1-n_3)^2} \quad (4)$$

Note that for a complete description including non-local densities, n and \mathbf{n}_v , as well as an analysis of the functionals, the reader is referred to the original references (Rosenfeld 1989).

The excess part of free energy due to the LJ attraction with respect to a hard-sphere reference fluid is defined by a density-weighted integral of a pair potential function over the surrounding fluids, separately summing the contributions from each species,

$$f_i^{LJ}(\mathbf{r}) = \sum_j \int_{1d}^{3.5d} 4\epsilon_{ij}^{LJ} \left[\left(\frac{d}{r} \right)^{12} - \left(\frac{d}{r} \right)^6 \right] \rho_j(\mathbf{r}') d\mathbf{r}' \quad (5)$$

where ϵ_{ij}^{LJ} is the LJ energy interaction parameter for fluid–fluid interaction potential, $\mathbf{r} = |\mathbf{s} - \mathbf{r}'|$ refers to the distance between particles i at position \mathbf{s} and j at \mathbf{r}' , and r is the cutoff distance. This contribution was considered to be within 1 to 3.5 molecular diameters, while it is set to zero outside this region.

The contribution to the free energy accounting for the short-range electrostatic interactions is expressed as

$$f_i^{MSA}(\mathbf{r}; \rho_i) = \sum_j \int_0^{1d} c_{ij}^{(2),el}(\mathbf{r}, \mathbf{r}') \rho_j(\mathbf{r}') d\mathbf{r}' \quad (6)$$

in which $c_{ij}^{(2),el}(\mathbf{r}, \mathbf{r}')$ is the cross-correlation between the Coulombic interaction and the hard-sphere exclusion, i.e. the electric residual part of the pair direct correlation function defined as the second functional derivative of the excess part of the free energy functional with respect to the single-particle density distribution (Hansen & McDonald 2006). It can be modeled with MSA (Waisman & Lebowitz 1972) for homogeneous systems, leading to

$$c_{ij,MSA}^{(2),el}(r) = \frac{q_i q_j e^2}{2\pi \epsilon_0 \epsilon_r} \left[\frac{B}{d} - \left(\frac{B}{d} \right)^2 \frac{r}{2} - \frac{1}{2r} \right], r < d \quad (7)$$

with the B parameter written as $B = \Gamma d / (1 + \Gamma d)$, where $\Gamma = \frac{\sqrt{1+2\kappa d} - d}{2d}$, $\kappa^2 = \frac{e^2}{\epsilon_0 \epsilon_r k_B T} \sum_i q_i^2 \rho_i^b$, ρ_i^b is the density of species i in bulk reservoir, q_i is the valence of the ionic species

i , and e is the elementary charge. The relative permittivity depends, in general, on the system temperature and composition.

RESULTS AND DISCUSSION

Fluid Structure at the Interface

The interaction parameters used in the f-DFT calculations are reported in Table 2. In the DFT/LJ-3CM results, the structural and thermodynamic properties such as density profiles, cation selectivity of ion exchange equilibrium, and free energy were fitted to reproduce atomistic simulations (Marry et al. 2008; Yang et al. 2017b), and the LJ energy parameters for fluid–fluid and wall–fluid were taken from molecular simulations (Magda et al. 1985; Lee et al. 2012). The uniform surface charge density in DFT//LJ-3CM was set to be the same as in MD simulations, -0.116 C/m^2 . To test the performance of the DFT/LJ-3CM in comparison with the DFT/HS-3CM, i.e. the solvent primitive model, the results for both approaches were compared with MD simulation for Mnt in the 10W hydrate state. HS radii used in the DFT/HS-3CM were the same as the LJ parameters in Table 2.

The DFT/LJ-3CM results taking into account the solvent effects were compared first with the atomic simulations for the case when Na-Mnt was saturated in a 0.62 M NaCl bulk solution. Density distributions were compared among water H_2O (i.e. water oxygen OW in MD simulations), Na^+ and Cl^- in the interlayer obtained with DFT/LJ-3CM, DFT/HS-3CM models, and atomic simulations (Fig. 2). The structured density profiles of interlayer water and ions from atomic simulations were predicted accurately by the DFT/LJ-3CM results. DFT/HS-3CM calculations overestimated, by nearly four times, the contact cation (Na^+) and water concentrations. The excessive cation density at the contact resulted in overcharging of the surface and values which were too large for co-adsorption of anions (e.g. Cl^-) at the interface. In the DFT/HS-3CM model, the solvent was modeled by neutral spheres instead of a

dielectric continuum as used in DFT/HS-2CM. Therefore, the wall/ion electrostatic interaction would be overestimated in the DFT/HS-3CM model and this could explain the overestimation of the densities at contact.

A similar comparison was conducted using the DFT/LJ-3CM model for Mnt saturated in a 0.23 M CaCl_2 bulk solutions for Ca-Mnt in the 10W hydration state. The density distributions of calcium and chloride ions and water molecules as a function of distance from the surface were obtained with the DFT/LJ-3CM model and from atomistic simulations. The DFT/LJ-3CM results agreed well with the atomistic simulations. The DFT/LJ-3CM model successfully captured the damped oscillations of Ca^{2+} and H_2O density distributions in the vicinity of the surface (Fig. 3). These important features were missing from the density profile obtained with the DFT/HS-2CM model. Furthermore, the number of density profiles of ionic and solvent molecules in the vicinity of the charged surface were substantially overestimated by the DFT/HS-3CM model. The mismatch of anion density predicted by the DFT/HS-3CM model in the 2:1 (e.g. CaCl_2) was even larger than in the 1:1 (e.g. NaCl) electrolyte. This can be explained by the stronger electrostatic effect of the Ca^{2+} ion compared to Na^+ . For the same (overestimated) cation atom density, Ca^{2+} resulted in stronger co-adsorption of Cl^- anions at the surface. The comparison demonstrated that the DFT/LJ-3CM model clearly performed better than the DFT/HS-3CM model near the fluid–wall interface, especially for 2:1 electrolytes. Accordingly, further comparison of results from the molecular simulation with the DFT/LJ-3CM model was restricted.

To test further the accuracy of the DFT/LJ-3CM model, the f-DFT results were compared with atomistic simulations of Na-Mnt in NaCl solution with various water contents, i.e. 2W, 3W, 4W, and 5W hydrated states (Holmboe & Bourg 2014; Yang et al. 2017b). The anions were essentially excluded from the nanopore when the distance between Mnt layers was $<10 \text{ \AA}$. The f-DFT results were insensitive to the bulk concentration of NaCl when the nanopore between Mnt layers was $<10 \text{ \AA}$. Accordingly, the concentration of bulk NaCl solutions

Table 2. The interaction energy parameters for the DFT/LJ-3CM simulation

Interaction energy parameter	$\text{Ca}^{2+} / \text{Na}^+$	DFT/LJ-3CM Cl^-	H_2O
Fluid–fluid interaction diameter d (\AA)	5.3 /4.848	4.25	2.5
Fluid–fluid ε_{ff}^{LJ} (eV)	0.006596	0.006596	0.006596
Fluid–fluid cut-off in r (\AA)	$3.5d$	$3.5d$	$3.5d$
Wall–fluid ε_{wf}^{LJ} (eV)	0.1351	0.1351	0.1351
Wall–fluid interaction diameter d (\AA)	5.3 /4.848	4.25	2.5
Wall–fluid cut-off in z (\AA)	$3.5d$	$3.5d$	$3.5d$
Relative permittivity ε_r ($T = 298 \text{ K}$)	--	--	78.3
Relative permittivity ε_r ($T = 323 \text{ K}$)	--	--	69.9
Relative permittivity ε_r ($T = 348 \text{ K}$)	--	--	62.4
Relative permittivity ε_r ($T = 373 \text{ K}$)	--	--	55.7

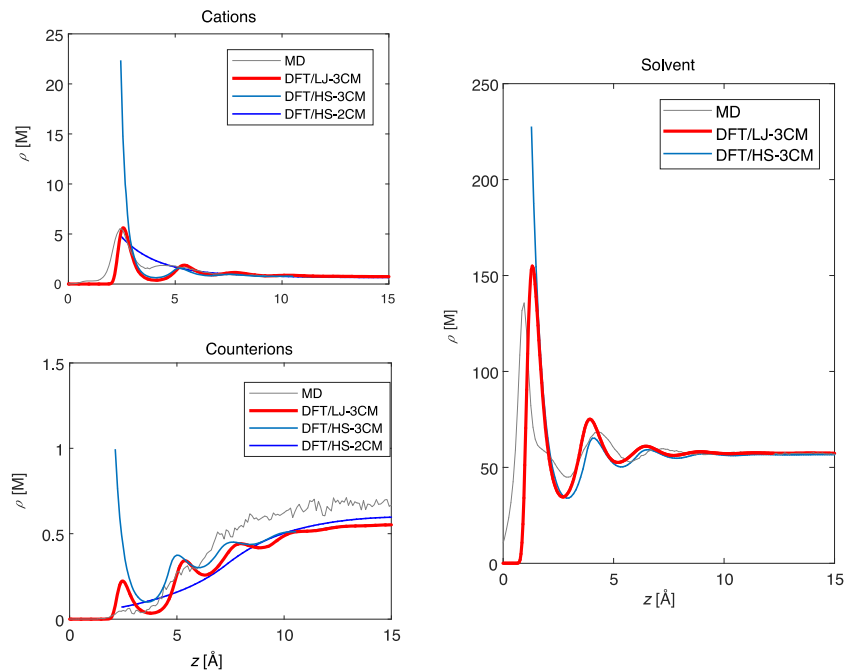


Fig. 2. Density distributions of Na^+ and Cl^- ions and H_2O from DFT/LJ-3CM calculations as a function of distance from the surface in the 10W hydration state. The DFT/LJ-3CM results are compared with atomic simulations (gray curves) and with calculations using the DFT/HS-3CM (blue curves) and DFT/HS-2CM (dark blue curves) models

in DFT calculations was set to be 0.6 M for Mnt in 2W, 3W, 4W, and 5W hydrated states.

The density profiles in a ~ 6.4 Å interlayer pore (Fig. 4) were obtained from the DFT/LJ-3CM model and atomistic

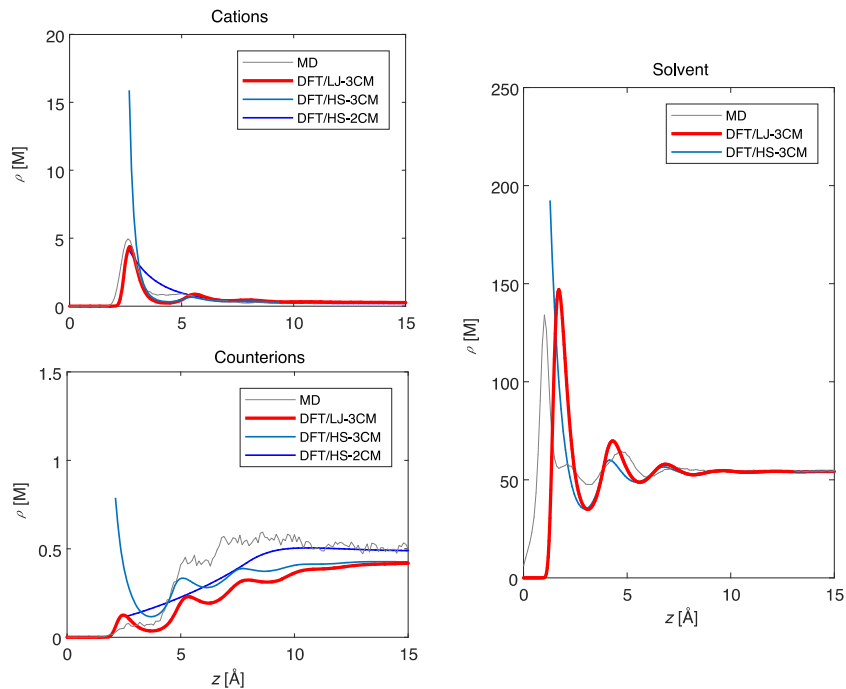


Fig. 3. Density distributions of Ca^{2+} , Cl^- ions, and H_2O from the DFT/LJ-3CM calculations as a function of distance from the surface in the 10W hydration state. The DFT/LJ-3CM results are compared with atomic simulations (gray curves) and with calculations using the DFT/HS-3CM (blue curves) and the DFT/HS-2CM (dark blue curves) models

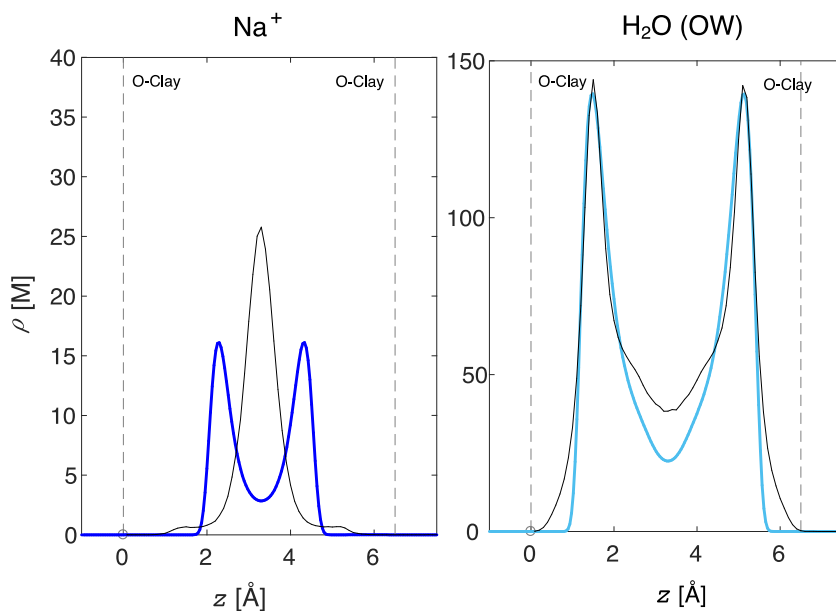


Fig. 4. Comparison of density distributions of Na^+ (dark blue) and water (light blue) predicted by the DFT/LJ-3CM model with atomic simulations (black curves) as a function of distance from the Mnt surface in 2W hydration state. The dashed gray lines represent the position of the outermost oxygen sites on the Mnt surface. The concentration of Cl^- ions was negligibly low and is not shown here for clarity

simulations corresponding to the 2W hydration state. The DFT/LJ-3CM model predicted two symmetrically peaked, cation-density profiles whereas atomistic simulations predicted single-peaked Na^+ density in the middle of the interlayer (Fig. 4). At such a low hydration state, the observed structuring of the fluid was controlled by the strong orientation-dependent ion–solvent and solvent–surface interactions. The observed difference was clear evidence that important features such as

H-bonding and rotation of water molecules were not taken into account by the DFT/LJ-3CM model.

Low temperature ion-dipole interaction cannot be captured by the orientation-independent LJ potential. However, the main features of water density distributions were captured successfully by the DFT/LJ-3CM results (Fig. 4). Atomistic simulations also indicated a small fraction of Na^+ forming a small local density maximum at ~ 1.5 Å from the surface.

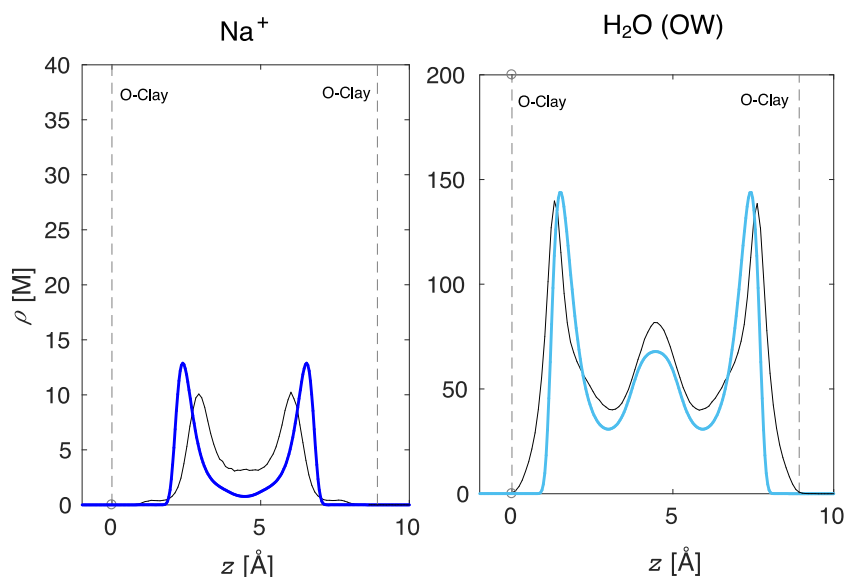


Fig. 5. Comparison of density distributions as a function of distance from the surface in the 3W hydration state from the DFT/LJ-3CM calculations (Na ion density is dark blue and H_2O density is light blue) with atomic simulations (black curves)

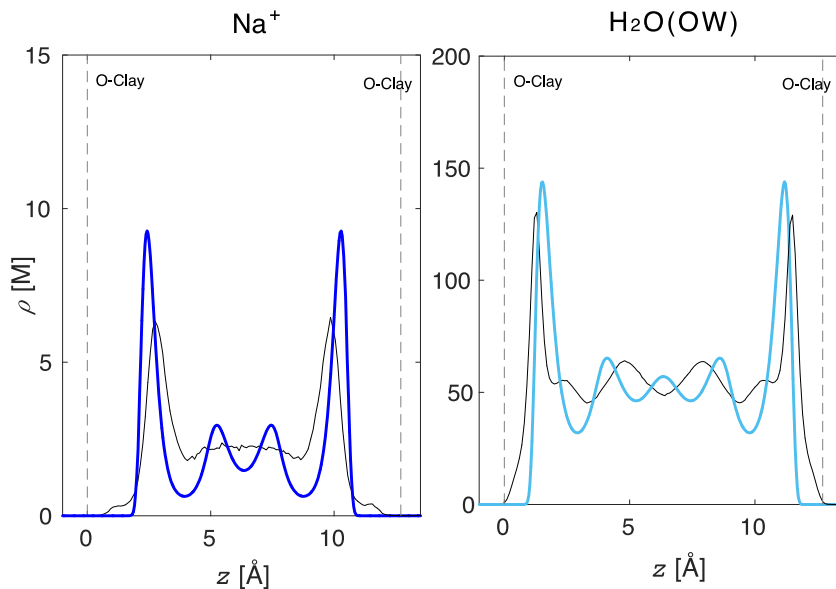


Fig. 6. Comparison of density distributions as a function of interlayer separations in the 4W hydration state obtained using the DFT/LJ-3CM model (Na ions are dark blue and H₂O is light blue) with atomic simulations (black curves)

These were inner-sphere complexes entering the hexagonal cavities of the tetrahedral sheet of Mnt. Such complexes were also present at the greater degrees of hydration discussed later. These features cannot be considered in the current DFT/LJ-3CM model which uses a simple planar interface.

The density distributions of calcium ions and water molecules in a ~ 9 Å interlayer pore were predicted by the DFT/LJ-3CM model and by atomistic simulations for Mnt in the 3W hydration state (Fig. 5). The DFT/LJ-3CM model captured the features of the density profiles of cations, especially the structure of interlayer water molecules in the 3W hydration state.

Again, Na and H₂O density profiles were predicted by the DFT/LJ-3CM model and the atomistic simulations of Mnt in the 4W hydrate state (Fig. 6). Similar Na and H₂O density profiles were predicted by the DFT/LJ-3CM model and the atomistic simulations for the 5W hydration state (Fig. 7). The density profiles of sodium ions predicted by the DFT/LJ-3CM model were more structured than profiles from MD simulations. Both the DFT/LJ-3CM results (blue curves) and the atomistic simulations (black curves) showed that Na⁺ ions were enriched at a distance of approximately $0.5d$ from the surface. This is comparable

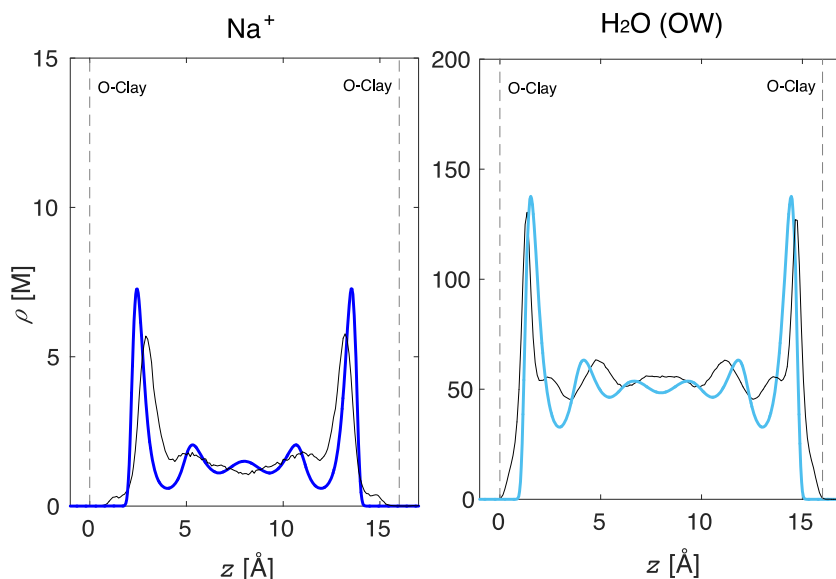


Fig. 7. Comparison of density distributions as a function of interlayer separations in the 5W hydration state from the DFT/LJ-3CM model (Na ions in dark blue and H₂O in light blue) with atomic simulations (black curves)

to the typical ion–surface distance of Na-outer-sphere complexes. As for the 3W state, DFT/LJ-3CM slightly over-predicted the structuring of the ion and water in the middle of the interlayer. The secondary features in the ions and water density distributions related to the non-planar surface topography were not reproduced by the f-DFT model. These secondary density maxima are related to partially hydrated inner-sphere Na ions entering the hexagonal cavities on the Mnt surface. Such a complex solvation behavior cannot be captured by the DFT/LJ-3CM model due to the over-simplistic planar representation of the surface and the lack of orientation-dependent ion–dipole interaction.

Overall analysis of the data demonstrated that the DFT/LJ-3CM model could capture the primary structural properties of ions and water in the vicinity of a fluid surface interface for very different hydration states of Mnt. The model tended to over-predict the structuring at greater distances from the surface in comparison with the MD simulation results. The features related to the non-planar interface and the changes in the hydration state of the ions, because of the changes from outer-sphere to the inner-sphere complexes, cannot be captured within the currently used DFT/LJ-3CM model.

Swelling Behavior

Depending on the chemical potential of water, smectite minerals are known to contain a distinct number of water molecules in the interlayer, commonly referred to as 1W, 2W, and 3W hydration states (Mooney et al. 1952; Karaborni et al. 1996; Kawamura et al. 1999). The stability of a particular hydration state and the exact interlayer thickness depends on temperature, composition of the electrolyte solution (both concentration and ion speciation in particular), and the distribution of isomorphous substitution in the TOT layer (Boek et al.

1995a,b; Young & Smith 2000; Hensen & Smit 2002; Smith et al. 2006; Tambach et al. 2006). A model-based description of smectite swelling is essential for prediction of a clay's mechanical properties (Hoang & Galliero 2015; Sun et al. 2015). The stable hydration state corresponds to the minimum value of the free energy of the system. The dependence of surface free energy, $\Omega(h)$, on the interlayer separation, h , is calculated by an integration of the solvation force via (Frink & van Swol 1998):

$$\Omega(h) - 2 * \Omega(\infty) = - \int_{\infty}^h dh' f_s(h') \quad (8)$$

The constant $\Omega(\infty)$ is equal to the surface free energy of an isolated wall in equilibrium with bulk fluid. The factor 2 in the left hand side of Eq. 8 accounts for the presence of two interfaces in the slit pore. The absolute minimum in $\Omega(h)$ determines the thermodynamically stable equilibrium separation of two walls, separated by h , for an unconstrained swelling condition, where the solvation force f_s is defined as $f_s = p - p_b$, and p is the total normal force per unit area on each wall, whereas p_b is the bulk pressure at the chosen chemical potential and temperature.

The dimensionless free energy of the system for Na- and Ca-Mnt was plotted as a function of slit pore size for various ionic strengths (Fig. 8). The symbol A in the vertical axis represents the surface area. Depending on the ionic strength of the external electrolyte, the stable states of the Ca and Na-Mnt predicted by DFT/LJ-3CM were either a dispersed one at lower ionic strength or a compacted “3W-Layer” state at higher ionic strength. The model for Na-Mnt predicted the dispersion to be stable if the bulk concentration of monovalent ions was < 2 M (Fig. 8a). The model for Ca-Mnt predicted the dispersion state

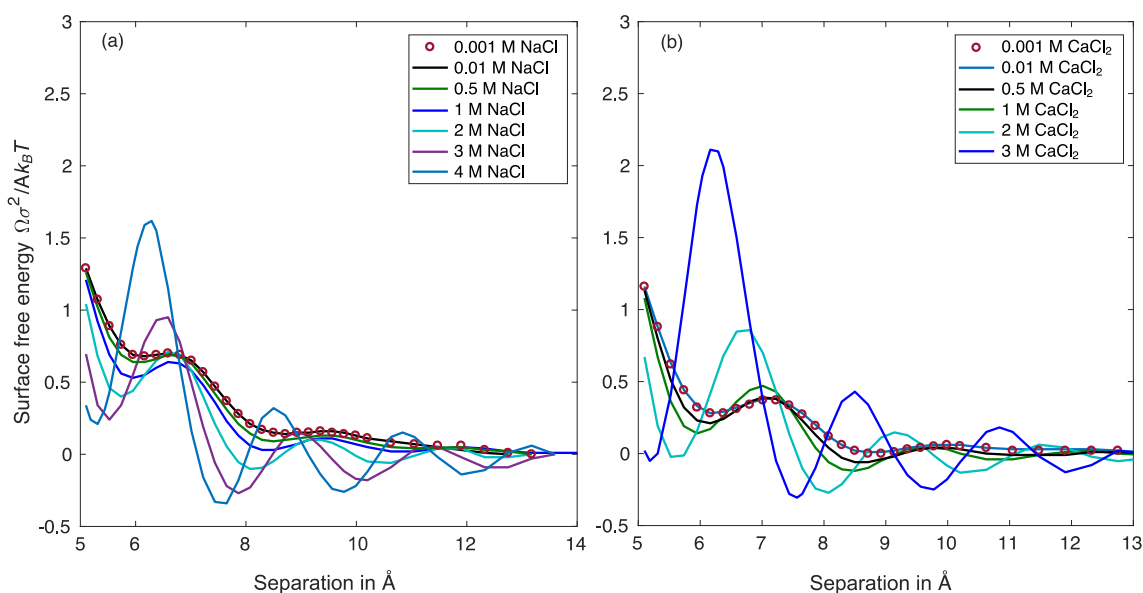
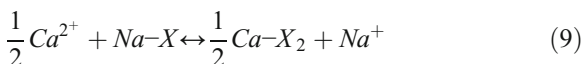


Fig. 8. Free energy per unit surface area as a function of the equilibrium interlayer separation between two smectite TOT layers in **a** NaCl, and **b** CaCl₂ bulk solutions. The ionic concentrations are indicated in the plots

to be stable at bulk concentrations of 2:1 electrolyte below 0.01 M (Fig. 8b). The metastable states with 2W and 4W layers were also apparent in the free energy profiles as local minima. The prediction of stable interlayer distances was based on changes in the chemical potential of each ion in the bulk electrolyte. The 2W state can become stable over the 3W state if the chemical potential of solute is further reduced, e.g. partial saturation (Churakov 2013). The behavior of the DFT/LJ-3CM for Mnt agreed very well qualitatively with the behavior of natural systems. The quantitative differences were related to the over-simplistic description of solvent and solvent–solute interactions, which were not captured in the model. Contrary to the experimental observations, Poisson-Boltzmann approximations predict repulsive interaction of Mnt platelets in NaCl and CaCl₂ solutions (Segad et al. 2010). The 2-component RPM model improved the predictions, suggesting an attractive force between TOT layers in Ca-Mnt at ~10 Å separation. In contrast to the DFT/LJ-3CM, the two-component RPM did not predict the existence of other, eventually metastable, hydration states. In this context the DFT/LJ-3CM model used in the present study clearly performed better than the widely used DFT-based description of swelling in clay minerals.

Thermodynamics of Ion Sorption

In this section, the DFT/LJ-3CM model was applied to evaluate ion exchange equilibrium and to estimate the effect of temperature on cation selectivity. The cation exchange between Ca²⁺ and Na⁺ ions in the interlayer of Mnt can be expressed by the following reaction (Appelo & Postma 2005):



where *X* indicates the clay mineral exchanger. The selectivity coefficient of ion exchange K_{GT} is given by the Gaines-

Thomas convention (Gaines & Thomas 1953; Appelo & Postma 2005) as

$$K_{GT} = \frac{[Na^+][Ca-X_2]^{0.5}}{[Ca^{2+}]^{0.5}[Na-X]} \quad (10)$$

where square brackets denote activities. $[Na^+]$ and $[Ca^{2+}]$ represent the activities of ions Na⁺ and Ca²⁺ in water, which can be related to the ion concentrations in bulk aqueous solutions. The surface activities $[Na-X]$ and $[Ca-X_2]$ are approximated by the equivalent charge fractions of Na⁺ and Ca²⁺ ions in the adsorbed phase in the DFT calculations. More detailed discussions of surface activities and ion exchange properties of clay minerals is available elsewhere (Yang et al. 2017a).

The selectivity coefficient K_{GT} as defined with the Gaines-Thomas convention was obtained by the DFT/LJ-3CM and the experimental results (Sposito et al. 1983) of the surface activities $[Na-X]$ i.e. $\beta_{Na} = \tau_{Na}/(\tau_{Na} + 2\tau_{Ca})$, where $\tau_i = \int_0^h (\rho_i(x) - \rho_i^b) dx$ (Table 3). The selectivity coefficients K_{GT} obtained previously using the DFT/HS-3CM model (Yang et al. 2017a) are shown for comparison.

To demonstrate the ability of the DFT/LJ-3CM to describe the cation exchange in Ca-Na-Mnt, the corresponding data in Table 3 were plotted (Figs. 9 and 10), and revealed (Fig. 9) the equivalent charge fractions of Na ions in the adsorbed phase, i.e. surface activities of Na-*X* (β_{Na}) from the experiments and the DFT/LJ-3CM calculations as a function of the mole fraction of Na ions in the mixture of NaCl and CaCl₂ bulk solutions. The calculations were performed at room and higher temperatures taking into account the change in the relative dielectric permittivity of water (Malmberg & Maryott 1956). The dielectric constant in the interlayer and in the bulk solution was assumed to have the same temperature dependence. The model predicted that temperature has a very limited effect on

Table 3. Thermodynamics of Ca-Na exchange in Wyoming Mnt predicted using the DFT/LJ-3CM model (present study), the DFT/HS-3CM model (Yang et al. 2017a), and the experimental data of Sposito et al. (1983)

Samples	$C_{Na}/(C_{Na}+C_{Ca})$	C_{Na} (mM)	C_{Ca} (mM)	DFT $K_{GT}(\sqrt{M})$		Experiments	
				LJ-3CM	HS-2CM	$K_{GT}(\sqrt{M})$	β_{Na}
01	97.9%	47.9	1.03	1.76	2.6	1.4	63.7%
02	96.1%	46.2	1.87	1.74	2.7	1.8	44.0%
03	93.5%	43.9	3.05	1.63	2.7	1.8	34.7%
04	90.4%	41.3	4.39	1.74	2.8	1.8	29.2%
05	85.0%	36.9	6.51	1.79	2.9	2.0	20.7%
06	77.4%	31.6	9.23	1.83	3.0	1.4	21.6%
07	69.7%	26.8	11.7	3.40	3.1	2.9	8.3%
08	61.4%	22.1	13.9	3.90	3.2	3.3	5.6%
09	51.1%	17.1	16.4	3.50	3.3	2.6	5.0%
10	39.4%	12.3	18.9	3.60	3.4	1.1	7.8%
11	22.2%	6.2	21.7	3.70	3.5	1.0	4.0%

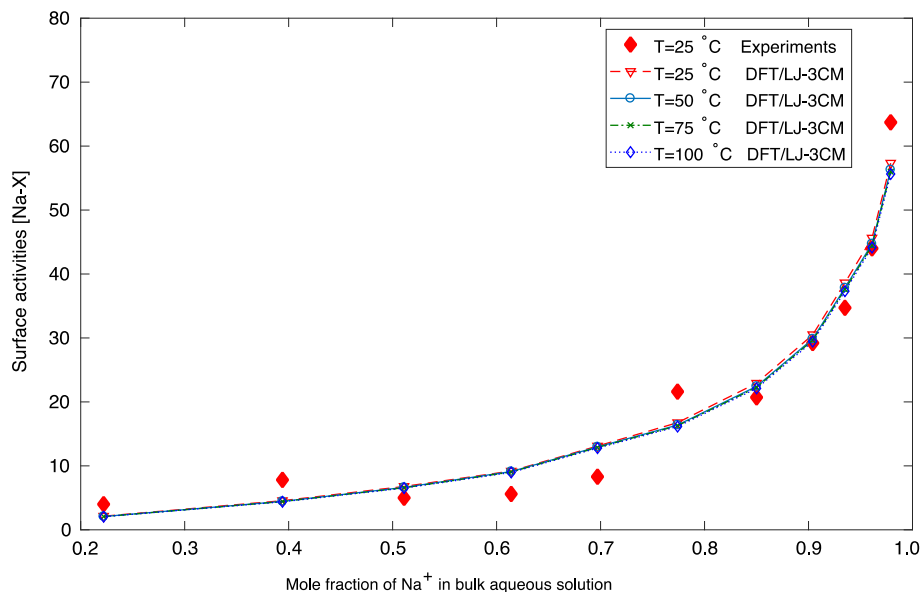


Fig. 9. Surface activities as a function of the mole fraction of Na^+ ions in the mixture of NaCl and CaCl_2 bulk electrolytes

the cation exchange in Na-Ca-Mnt . Na sorption decreased only slightly with increasing temperature. The comparison of *f*-DFT calculations and experiments showed that the DFT/LJ-3CM model can quantitatively and qualitatively reproduce the measurements of cation exchange for Mnt in the Na and Ca electrolyte solutions.

The selectivity coefficient K_{GT} from the DFT calculations and measurements, represented as a function of the mole fraction of NaCl in the mixture of NaCl and CaCl_2 bulk solutions using the DFT/LJ-3CM (Fig. 10), revealed a distinct advantage over the RPM calculations in comparison with the experimental results (Sposito et al. 1983). The DFT/LJ-3CM results agreed quite well

with the experiments when the mole fraction of Na ions in the bulk was >0.4 . The interlayer separations in the *f*-DFT calculations of the selectivity coefficient were set at 30 \AA when Na was dominant (i.e. Na mole fraction >0.7), which is commonly used in simulations for pure Na electrolyte solutions because the Mnt layers tend to disperse. However, the Mnt layers collapsed and formed a gel with $\sim 9 \text{ \AA}$ interlayer separation (the compacted ‘3W-Layer’ state) for Ca salts with bulk ion concentration $\geq 10 \text{ mM}$ (Fig. 8). Accordingly, the interlayer separations in the DFT calculations were set to be 9 \AA when Ca was dominant in the bulk solutions (i.e. Na mole fraction <0.7). The selectivity coefficient $\log_{10}K_{GT}$ (Fig. 11) was plotted as a function of the Na charge

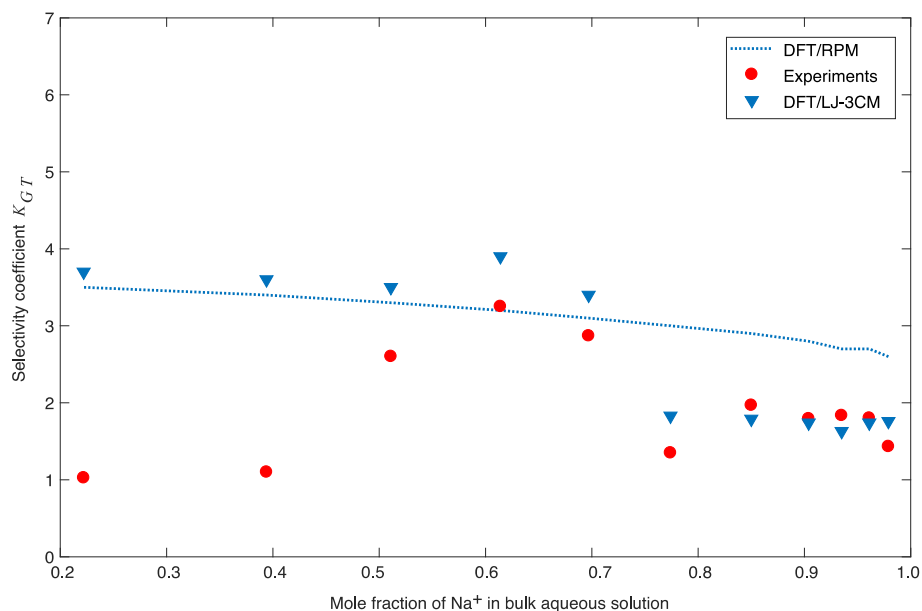


Fig. 10. The selectivity coefficient K_{GT} as a function of the mole fraction of Na ions in the mixture of NaCl and CaCl_2 bulk solution

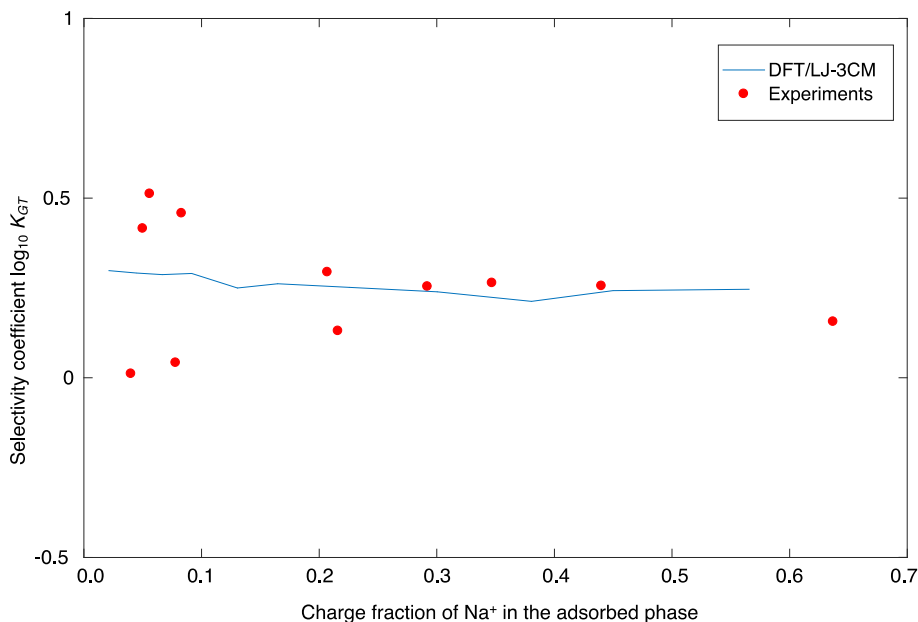


Fig. 11. The selectivity coefficient, $\log_{10}K_{GT}$, as a function of the charge fraction of the Na^+ ions in the adsorbed phase. The curve shows the DFT results. The solid dots represent the experimental data from Sposito et al. (1983)

fraction at the surface, i.e. the surface activities in the adsorbed phase. A linear relationship consistent with the experimental observations was recovered between the selectivity coefficient and the surface activities.

SUMMARY AND CONCLUSIONS

The accurate description of fluid–solid interface structure and the thermodynamics of the diffuse double layer (e.g. ionic concentration profiles and ionic mobility as a function of distance from the surface) is indispensable for accurate modeling of ion transport and retention in compacted clay systems (van Schaik et al. 1966; Gimmi & Kosakowski 2011). These model parameters can be obtained, in principle, by full-scale atomistic simulations. The direct application of MD simulation to near-reality systems representing complex networks of pores in clays is currently not feasible due to the high computational costs (Churakov & Gimmi 2011; Churakov et al. 2014). Widely used and computationally efficient RPM models of electrolyte on the other hand ignore the molecular nature of the solvent and fail to provide good quantitative description of the ion and solvent profiles close to the solid interface due to the simplistic nature of the underlying interaction potential. Application of three component *tf*-DFT models for electrolytes, which take into account soft ions and solvent, could be a powerful way to obtain accurate molecular-scale descriptions of mineral–electrolyte interfaces at comparatively low computational costs.

In the present work, the performance of the three-component DFT/LJ-3CM model was tested against full-scale molecular simulation of Na and Ca Mnt in various hydration states. In good agreement with the atomistic simulation, the DFT/LJ-3CM model reproduced accurately the short-range

structuring of the ions and solvent molecules at TOT layer separations >10 Å. In very narrow slit pores of <10 Å, the solvent structure was reasonably reproduced. Under these conditions, the molecular system behavior was controlled by orientation-dependent ion-dipole interaction and hydrogen bonding. Furthermore, the real clay surface has a complex 3-dimensional arrangement of oxygen atoms, allowing ion-specific steric interaction, whereas the *f*-DFT model assumes a planar interface. These coordination-dependent interactions and the molecular nature of the surface were not taken into account properly in the current model.

The DFT/LJ-3CM model was further applied to evaluate swelling behavior of Ca and Na Mnt and the Na-Ca exchange equilibrium. The calculations of selectivity coefficients for Na-Ca exchange reactions agreed well with experimental observations. The swelling behavior of DFT/LJ-3CM Mnt was in good qualitative agreement with the experimental observations. Exceptionally, the model predicted local free energy minima of the system for discrete 1W, 2W, and 3W hydration states. The DFT/LJ-3CM model is clearly superior to conventional 3CM and RPM in predicting solvent structure and the thermodynamics of DDL.

The DFT/LJ-3CM calculations were at least 3–4 orders of magnitude less demanding in terms of computational resources compared to conventional MD simulations. The DFT/LJ-3CM model applied in this work was able to describe the cation selectivity of ion exchange equilibrium in a wide range of solution compositions. Such a model can be used in reactive transport simulators and modeling ion migration taking place under more complex thermo-chemo-hydro-mechanical conditions. The ability of the DFT/LJ-3CM model to capture the water and ion density distributions is of great interest for many practical applications such as upscaling of the results to pore-level for reactive transport simulations in porous media. The *f*-DFT tool provides a more

computationally economic way to achieve those goals because of its ability to model simple fluid systems of increased complexity, e.g. 3D systems not restricted to system size. The computational advantage of f-DFT allows researchers to execute rapid parametric studies (parameters: pore-size/solution concentration) and can bridge between atomistic and pore-level simulations.

ACKNOWLEDGMENTS

The authors acknowledge financial support by the Marie Skłodowska-Curie Actions, MSCA-COFUND, PSI-FELLOW-II-3i grant agreement No. 701647. The atomistic simulations were performed using resources provided by the Swiss Center of Scientific Computing (CSCS) for High Performance Computing. The authors are grateful to Dr Michael Holmboe for discussions about the MD simulations and to Dr Pflingsten Wilfried for discussions on cation adsorption on mineral surfaces.

Compliance with Ethical Standards

Conflict of Interest

The authors declare that they have no conflict of interest.

REFERENCES

- Alt-Epping, P., Gimmi, T., Wersin, P., & Jenni, A. (2018). Incorporating electrical double layers into reactive-transport simulations of processes in clays by using the Nernst-Planck equation: A benchmark revisited. *Applied Geochemistry*, *89*, 1–10.
- Appelo, C.A.J., & Postma, D. (2005). Ion exchange. Pp. 241–309 in: *Geochemistry, Groundwater and Pollution*. Taylor & Francis. doi: <https://doi.org/10.1201/9781439833544.ch6>
- Åqvist, J. (1990). Ion-water interaction potentials derived from free energy perturbation simulations. *The Journal of Physical Chemistry*, *94*, 8021–8024.
- Berendsen, H. J. C., Postma, J. P. M., van Gunsteren, W. F., DiNola, A., & Haak, J. R. (1984). Molecular dynamics with coupling to an external bath. *The Journal of Chemical Physics*, *81*, 3684–3690.
- Berendsen, H. J. C., Grigera, J. R., & Straatsma, T. P. (1987). The missing term in effective pair potentials. *The Journal of Physical Chemistry*, *91*, 6269–6271.
- Berendsen, H. J. C., van der Spoel, D., & van Drunen, R. (1995). GROMACS: a message-passing parallel molecular dynamics implementation. *Computer Physics Communications*, *91*, 43–56.
- Bloom, P.R. (2000). Soil pH and pH buffering. Pp. B333–B352 in: *Handbook of Soil Science. Section B Soil Chemistry* (M.E. Sumner, editor). CRC Press: Boca Raton, Florida, USA.
- Boda, D., Henderson, D., Plaschko, P., & Fawcett, W. R. (2004). Monte Carlo and density functional theory study of the electrical double layer: the dependence of the charge/voltage relation on the diameter of the ions. *Molecular Simulation*, *30*, 137.
- Boek, E. S., Coveney, P. V., & Skipper, N. T. (1995a). Molecular modeling of clay hydration: A study of hysteresis loops in the swelling curves of sodium montmorillonites. *Langmuir*, *11*, 4629–4631.
- Boek, E. S., Coveney, P. V., & Skipper, N. T. (1995b). Monte Carlo Molecular modeling studies of hydrated Li-, Na-, and K-Smectites: Understanding the role of potassium as a clay swelling inhibitor. *Journal of the American Chemical Society*, *117*, 12608–12617.
- Botan, A., Rotenberg, B., Marry, V., Turq, P., & Noetinger, B. (2011). Hydrodynamics in Clay Nanopores. *The Journal of Physical Chemistry C*, *115*, 16109–16115.
- Botan, A., Marry, V., Rotenberg, B., Turq, P., & Noetinger, B. (2013). How electrostatics influences hydrodynamic boundary conditions: Poiseuille and electro-osmotic flows in clay nanopores. *The Journal of Physical Chemistry C*, *117*, 978–985.
- Bourg, I. C., & Sposito, G. (2011). Molecular dynamics simulations of the electrical double layer on smectite surfaces contacting concentrated mixed electrolyte (NaCl-CaCl₂) solutions. *Journal of Colloid and Interface Science*, *360*, 701–715.
- Bourg, I. C., Bourg, A. C. M., & Sposito, G. (2003). Modeling diffusion and adsorption in compacted bentonite: a critical review. *Journal of Contaminant Hydrology*, *61*, 293–302.
- Chang, F. R. C., Skipper, N. T., & Sposito, G. (1998). Monte Carlo and molecular dynamics simulations of electrical double-layer structure in potassium-montmorillonite hydrates. *Langmuir*, *14*, 1201–1207.
- Churakov, S. V. (2013). Mobility of Na and Cs on montmorillonite surface under partially saturated conditions. *Environmental Science & Technology*, *47*, 9816–9823.
- Churakov, S. V., & Gimmi, T. (2011). Up-scaling of molecular diffusion coefficients in clays: A two-step approach. *The Journal of Physical Chemistry C*, *115*, 6703–6714.
- Churakov, S. V., Gimmi, T., Unruh, T., Loon, L. R. V., & Juranyi, F. (2014). Resolving diffusion in clay minerals at different time scales: Combination of experimental and modeling approaches. *Applied Clay Science*, *96*, 36–44.
- Cygan, R. T., Liang, J. J., & Kalinichev, A. G. (2004). Molecular models of hydroxide, oxyhydroxide, and clay phases and the development of a general force field. *The Journal of Physical Chemistry B*, *108*, 1255–1266.
- Darden, T., York, D., & Pederson, L. (1993). Particle mesh Ewald: An N-log(N) method for Ewald sums in large systems. *The Journal of Chemical Physics*, *98*, 10089.
- Edil, T. B. (2003). A review of aqueous-phase VOC transport in modern landfill liners. *Waste Management*, *24*, 561–571.
- Eriksen, T. E., Jansson, M., & Molera, M. (1999). Sorption effects on cation diffusion in compacted bentonite. *Engineering Geology*, *54*, 231–236.
- Fenter, P., Cheng, L., Rihs, S., Machesky, M., Bedzyk, M. J., & Sturchio, N. C. (2000). Electrical double-layer structure at the rutile-water interface as observed in situ with small-period X-ray standing waves. *Journal of Colloid and Interface Science*, *225*, 154–165.
- Frink, L. J. D., & van Swol, F. (1998). Solvation forces between rough surfaces. *The Journal of Chemical Physics*, *108*, 5588.
- Gaines Jr., G. L., & Thomas, H. C. (1953). Adsorption studies on clay minerals. II. A formulation of the thermodynamics of exchange adsorption. *The Journal of Chemical Physics*, *21*, 714.
- Gimmi, T., & Churakov, S. V. (2019). Water retention and diffusion in unsaturated clays: Connecting atomistic and pore scale simulations. *Applied Clay Science*, *175*, 169–183.
- Gimmi, T., & Kosakowski, G. (2011). How mobile are sorbed cations in clays and clay rocks? *Environmental Science & Technology*, *45*, 1443–1449.
- Hansen, J.-P., & McDonald, I. R. (2006). *Theory of Simple Liquids*. London: Academic Press.
- Henderson, D. (Ed.). (1992). *Fundamentals of Inhomogeneous Fluids*. New York: Marcel Dekker, Inc.
- Hensen, E. J. M., & Smit, B. (2002). Why clays swell. *The Journal of Physical Chemistry B*, *106*, 12664–12667.
- Hoang, H., & Galliero, G. (2015). Couplings between swelling and shear in saturated slit nanopores: A molecular simulation study. *Physical Review E*, *91*, 012401.
- Holmboe, M., & Bourg, I. C. (2014). Molecular dynamics simulations of water and sodium diffusion in smectite interlayer nanopores as a function of pore size and temperature. *The Journal of Physical Chemistry C*, *118*, 1001–1013.
- Jeanmairat, G., Marry, V., Levesque, M., Rotenberg, B., & Borgis, D. (2014). Hydration of clays at the molecular scale: the promising perspective of classical density functional theory. *Molecular Physics*, *112*, 1320–1329.
- Jorgensen, W. L., Chandrasekhar, J., Madura, J. D., Impey, R. W., & Klein, M. L. (1983). Comparison of simple potential functions for

- simulating liquid water. *The Journal of Chemical Physics*, 79, 926–935.
- Joung, I. S., & Cheatham III, T. E. (2008). Determination of alkali and halide monovalent ion parameters for use in explicitly solvated biomolecular simulations. *The Journal of Physical Chemistry B*, 112, 9020–9041.
- Karaborni, S., Smit, B., Heidug, W., Urai, J., & Oort, E. V. (1996). The swelling of clays: Molecular simulations of the hydration of montmorillonite. *Science*, 271, 1102–1104.
- Kawamura, K., Ichikawa, Y., Nakano, M., Kitayama, K., & Kawamura, H. (1999). Swelling properties of smectite up to 90°C. In situ X-ray diffraction experiments and molecular dynamic simulations. *Engineering Geology*, 54, 75–79.
- Kosakowski, G., Churakov, S. V., & Thoenen, T. (2008). Diffusion of Na and Cs in montmorillonite. *Clays and Clay Minerals*, 56, 190–206.
- Lamperski, S., & Zydor, A. (2007). Monte Carlo study of the electrode|solvent primitive model electrolyte interface. *Electrochimica Acta*, 52, 2429–2436.
- Lee, J. W., Nilson, R. H., Templeton, J. A., Griffiths, S. K., Kung, A., & Wong, B. M. (2012). Comparison of molecular dynamics with classical density functional and poisson-boltzmann theories of the electric double layer in nanochannels. *Journal of Chemical Theory and Computation*, 8, 2012–2022.
- Lee, J. W., Templeton, J. A., Mandadapu, K. K., & Zimmerman, J. A. (2013). Comparison of molecular and primitive solvent models for electrical double layers in nanochannels. *Journal of Chemical Theory and Computation*, 9, 3051–3061.
- Lian, C., Zhan, C., Jiang, D., Liu, H., & Wu, J. (2017). Capacitive energy extraction by few-layer graphene electrodes. *The Journal of Physical Chemistry C*, 121, 14010–14018.
- Lo, I. M. C., Mak, R. K. M., & Lee, S. C. H. (1997). Modified clays for waste containment and pollutant attenuation. *Journal of Environmental Engineering*, 123, 25–32.
- Magda, J. J., Tirrell, M., & Davis, H. T. (1985). Molecular dynamics of narrow, liquid-filled pores. *The Journal of Chemical Physics*, 83, 1888–1901.
- Malmberg, C. G., & Maryott, A. A. (1956). Dielectric constant of water from 0° to 100°C. *Journal of Research of the National Institute of Standards and Technology*, 56, 1–8.
- Marry, V., Rotenberg, B., & Turq, P. (2008). Structure and dynamics of water at a clay surface from molecular dynamics simulation. *Physical Chemistry Chemical Physics*, 10, 4802.
- Marschall, P., Horseman, S., & Gimmi, T. (2005). Characterisation of gas transport properties of the Opalinus Clay, a potential host rock formation for radioactive waste disposal. *Oil & Gas Science and Technology*, 60, 121–139.
- Melkior, T., Yahiaoui, S., Motellier, S., Thoby, D., & Tevissen, E. (2005). Cesium sorption and diffusion in Bure mudrock samples. *Applied Clay Science*, 29, 172–186.
- Melkior, T., Yahiaoui, S., Thoby, D., Motellier, S., & Barthes, V. (2007). Diffusion coefficients of alkaline cations in Bure mudrock. *Physics and Chemistry of the Earth*, 32, 453–462.
- Mooney, R. W., Keenan, A. G., & Wood, L. A. (1952). Adsorption of water vapor by montmorillonite. II. Effect of exchangeable ions and lattice swelling as measured by X-Ray diffraction. *Journal of the American Chemical Society*, 74, 1371–1374.
- Moucka, F., Svoboda, M., & Lisal, M. (2017). Modelling aqueous solubility of sodium chloride in clays at thermodynamic conditions of hydraulic fracturing by molecular simulations. *Physical Chemistry Chemical Physics*, 19, 16586–16599.
- Obliger, A., Duval, M., Jardat, M., Coelho, D., Bekri, S., & Rotenberg, B. (2013). Numerical homogenization of electrokinetic equations in porous media using lattice-Boltzmann simulations. *Physical Review E*, 88, 013019.
- Obliger, A., Jardat, M., Coelho, D., Bekri, S., & Rotenberg, B. (2014). Pore network model of electrokinetic transport through charged porous media. *Physical Review E*, 89, 043013.
- Oleksy, A., & Hansen, J. P. (2010). Wetting of a solid substrate by a “civilized” model of ionic solutions. *The Journal of Chemical Physics*, 132, 204702.
- Pagonabarraga, I., Rotenberg, B., & Frenkel, D. (2010). Recent advances in the modelling and simulation of electrokinetic effects: bridging the gap between atomistic and macroscopic descriptions. *Physical Chemistry Chemical Physics*, 12, 9566–9580.
- Prasianakis, N., Curti, I. E., Kosakowski, G., Poonosamy, J., & Churakov, S. V. (2017). Deciphering pore-level precipitation mechanisms. *Scientific Reports*, 7, 13765.
- Price, D. J., & Brooks, C. L. (2004). A modified TIP3P water potential for simulation with Ewald summation. *The Journal of Chemical Physics*, 121, 10096–10103.
- Qiao, R., & Aluru, N. R. (2003). Ion concentrations and velocity profiles in nanochannel electroosmotic flows. *The Journal of Physical Chemistry*, 118, 4692–4701.
- Rosenfeld, Y. (1989). Free-energy model for the inhomogeneous hard-sphere fluid mixture and density-functional theory of freezing. *Physical Review Letters*, 63, 980.
- Rotenberg, B., Marry, V., Dufreche, J. F., Malikova, N., Giffaut, E., & Turq, P. (2007a). Modelling water and ion diffusion in clays: A multiscale approach. *Comptes Rendus Chimie*, 10, 1108.
- Rotenberg, B., Marry, V., Dufreche, J.-F., Giffaut, E., & Turq, P. (2007b). A multiscale approach to ion diffusion in clays: Building a two-state diffusion-reaction scheme from microscopic dynamics. *Journal of Colloid and Interface Science*, 309, 289–295.
- Rowe, R. K. (2005). Long-term performance of contaminant barrier systems. *Geotechnique*, 55, 631–678.
- Schaettle, K., Pestana, L. R., Head-Gordon, T., & Lammers, L. N. (2018). A structural coarse-grained model for clays using simple iterative Boltzmann inversion. *The Journal of Chemical Physics*, 148, 222809.
- Schlegel, M. L., Nagy, K. L., Fenter, P., Cheng, L., Sturchio, N. C., & Jacobsen, S. D. (2006). Cation sorption on the muscovite (0 0 1) surface in chloride solutions using high-resolution X-ray reflectivity. *Geochimica et Cosmochimica Acta*, 70, 3549–3565.
- Schoonheydt, R. A., & Johnston, C. (2006). Surface and interface chemistry of clay minerals. Pp. 139–165 in: *Handbook of Clay Science, Volume 1* (F. Bergaya, B.K.G. Theng, & G. Lagaly editors). 1st Edition. Elsevier Science.
- Segad, M., Jonsson, B., Akesson, T., & Cabane, B. (2010). Ca/Na montmorillonite: Structure, forces and swelling properties. *Langmuir*, 26, 5782–5790.
- Silvestre-Alcantara, W., Kaja, M., Henderson, D., Lamperski, S., & Bhuiyan, L. B. (2016). Structure and capacitance of an electric double layer formed by fused dimer cations and monomer anions: a Monte Carlo simulation study. *Molecular Physics*, 114, 53–60.
- SKB. Swedish Nuclear Fuel and Waste Management Co. (2006). Long-term safety for KBS-3 repositories at Forsmark and Laxemar – a first evaluation. *SKB Technical Report*, TR-06-09.
- Skipper, N. T., Chang, F. R. C., & Sposito, G. (1995a). Monte-Carlo simulation of interlayer molecular-structure in swelling clay-minerals. 1. Methodology. *Clays and Clay Minerals*, 43, 285–293.
- Skipper, N. T., Chang, F. R. C., & Sposito, G. (1995b). Monte Carlo simulation of interlayer molecular structure in swelling clay minerals. 2. Monolayer hydrates. *Clays and Clay Minerals*, 43, 294–303.
- Smith, D. E., Wang, Y., Chaturvedi, A., & Whitley, H. D. (2006). Molecular simulations of the pressure, temperature, and chemical potential dependencies of clay swelling. *The Journal of Physical Chemistry B*, 110, 20046–20054.
- Song, J., & Zhang, D. (2013). Comprehensive review of caprock-sealing mechanisms for geologic carbon sequestration. *Environmental Science & Technology*, 47, 9–22.
- Sposito, G. (1984). *The Surface Chemistry of Soils*. New York: Oxford University Press.
- Sposito, G., Holtzclaw, K. M., Charlet, L., Jouany, C., & Page, A. L. (1983). Sodium-calcium and sodium-magnesium exchange on Wyoming bentonite in perchlorate and chloride background ionic media. *Soil Science Society of America Journal*, 47, 51–56.

- Sun, L. L., Hirvi, J. T., Schatz, T., Kasa, S., & Pakkanen, T. A. (2015). Estimation of montmorillonite swelling pressure: A molecular dynamics approach. *The Journal of Physical Chemistry C*, *119*, 19863–19868.
- Tambach, T. J., Hensen, E. J. M., & Smit, B. (2004). Molecular simulations of swelling clay minerals. *The Journal of Physical Chemistry B*, *108*, 7586–7596.
- Tambach, T. J., Bolhuis, P. G., Hensen, E. J. M., & Smit, B. (2006). Hysteresis in clay swelling induced by hydrogen bonding: Accurate prediction of swelling states. *Langmuir*, *22*, 1223–1234.
- Tang, Z., Scriven, L. E., & Davis, H. T. (1991). Density-functional perturbation theory of inhomogeneous simple fluids. *The Journal of Chemical Physics*, *95*, 2659.
- Tang, Z., Scriven, L. E., & Davis, H. T. (1992). A three-component model of the electrical double layer. *The Journal of Chemical Physics*, *97*, 494.
- Torrie, G. M., & Valleau, J. P. (1980). Electrical double layers. I. Monte Carlo study of a uniformly charged surface. *The Journal of Chemical Physics*, *73*, 5807.
- Tournassat, C., Chapron, Y., Leroy, P., Bizi, M., & Boulahya, F. (2009). Comparison of molecular dynamics simulations with triple layer and modified Gouy–Chapman models in a 0.1 M NaCl–montmorillonite system. *Journal of Colloid and Interface Science*, *339*, 533–541.
- Tyagi, M., Gimmi, T., & Churakov, S. V. (2013). Multi-scale microstructure generation strategy for up-scaling transport in clays. *Advances in Water Resources*, *59*, 181–195.
- van der Spoel, D., Lindahl, E., Hess, B., Groenhof, G., Mark, A. E., & Berendsen, H. J. C. (2005). GROMACS: fast, flexible, and free. *Journal of Computational Chemistry*, *26*, 1701–1718.
- van Loon, L. R., & Eikenberg, J. (2005). A high-resolution abrasive method for determining diffusion profiles of sorbing radionuclides in dense argillaceous rocks. *Applied Radiation and Isotopes*, *63*, 11–21.
- van Schaik, J. C., Kemper, W. D., & Olsen, S. R. (1966). Contribution of adsorbed cations to diffusion in clay-water systems. *Soil Science Society of America Journal*, *30*, 17–22.
- Waisman, E., & Lebowitz, J. L. (1972). Mean spherical model integral equation for charged hard spheres I. Method of solution. *The Journal of Chemical Physics*, *56*, 3086–3093.
- Yang, G., & Liu, L. (2015). A systematic comparison of different approaches of density functional theory for the study of electrical double layers. *The Journal of Chemical Physics*, *142*, 194110.
- Yang, G., Neretnieks, I., Moreno, L., & Wold, S. (2016). Density functional theory of electrolyte solutions in slit-like nanopores II. Applications to forces and ion exchange. *Applied Clay Science*, *132–133*, 561–570.
- Yang, G., Neretnieks, I., Moreno, L., & Wold, S. (2017a). Density functional theory of electrolyte solutions in slit-like nanopores I. The RFD/WCA approach extended to non-restricted primitive model. *Applied Clay Science*, *135*, 526–531.
- Yang, G., Neretnieks, I., & Holmboe, M. (2017b). Atomistic simulations of cation hydration in sodium and calcium montmorillonite nanopores. *The Journal of Chemical Physics*, *147*, 084705.
- Yang, Y., Patel, R. A., Churakov, S. V., Prasianakis, N. I., Kosakowski, G., & Wang, M. (2019). Multiscale modeling of ion diffusion in cement paste: electrical double layer effects. *Cement and Concrete Composites*, *96*, 55–65.
- Young, D. A., & Smith, D. E. (2000). Simulations of clay mineral swelling and hydration: Dependence upon interlayer ion size and charge. *The Journal of Physical Chemistry B*, *104*, 9163–9170.

(Received 16 August 2019; Revised 16 December 2019; AE: Andrey G. Kalinichev)